Biochimica et Biophysica Acta 1808 (2011) 2849–2858

Contents lists available at SciVerse ScienceDirect

Biochimica et Biophysica Acta

journal homepage: www.elsevier.com/locate/bbamem

Correlation between the ripple phase and stripe domains in membranes

Uffe Bernchou [1], Henrik Midtiby [2], John Hjort Ipsen, Adam Cohen Simonsen *

MEMPHYS-Center for Biomembrane Physics, Department of Physics and Chemistry, University of Southern Denmark, 5230 Odense M, Denmark

ARTICLE INFO

Article history:
Received 25 May 2011
Received in revised form 12 August 2011
Accepted 16 August 2011
Available online 24 August 2011

Keywords:
Supported lipid bilayer
Ripple phase
Stripe phase
Solid phase
AFM
Fluorescence microscopy

ABSTRACT

We investigate the relationship between stripe domains and the ripple phase in membranes. These have previously been observed separately without being linked explicitly. Past results have demonstrated that solid and ripple phases exhibit rich textural patterns related to the orientational order of tilted lipids and the orientation of ripple corrugations. Here we reveal a highly complex network pattern of ripple and solid domains in DLPC, DPPC bilayers with structures covering length scales from 10 nm to 100 μm. Using spincoated double supported membranes we investigate domains by correlated AFM and fluorescence microscopy. Cooling experiments demonstrate the mode of nucleation and growth of stripe domains enriched in the fluorescent probe. Concurrent AFM imaging reveals that these stripe domains have a one-to-one correspondence with a rippled morphology running parallel to the stripe direction. Both thin and thick stripe domains are observed having ripple periods of 13.5 ± 0.2 nm and 27.4 ± 0.6 nm respectively. These are equivalent to previously observed asymmetric/equilibrium and symmetric/metastable ripple phases, respectively. Thin stripes grow from small solid domains and grow predominantly in length with a speed of ~3 times that of the thick stripes. Thick stripes grow by templating on the sides of thinner stripes or can emerge directly from the fluid phase. Bending and branching angles of stripes are in accordance with an underlying six fold lattice. We discuss mechanisms for the nucleation and growth of ripples and discuss a generic phase diagram that may partly rationalize the coexistence of metastable and stable phases.

1. Introduction

Model membranes provide a platform for understanding domains in biomembranes in terms of thermodynamics and soft condensed matter concepts [1]. Membranes with a few lipid components can display remarkably rich thermodynamic behavior and exhibit complex domain morphologies. An interesting example is the ripple phase characterized by periodic corrugations in the lipid bilayer. For pure lipids it is stable in a narrow temperature range and ripples can generally exist in several metastable forms. The ripple phase is formed by a very wide range of membrane lipids including phosphatidylcholines, phosphatidylglycerol and sphingomyelin in the temperature interval between the pretransition and the main phase transition [2,3]. Currently the ripple phase is not known to have biological significance, but its abundance in model systems is intriguing and calls for a deeper understanding. Since its discovery [4–6], the ripple phase has been extensively studied by various experimental techniques including freeze-fracture electron microscopy [3,7,8], scanning tunneling microscopy [9], X-ray scattering [2,10–15], neutron scattering [16], NMR spectroscopy [17], and ESR spectroscopy [18]. Several theoretical models have been proposed to explain the formation of the ripple structure [19–25].

The emergence of ripples is closely associated with the main phase transition. In [25,26] it was demonstrated by the use of the simplest possible model of the chain melting transition in a flexible bilayer that the formation of two rippled structures with periodicity which differs by a factor of 2 is expected when the intermonolayer coupling is weak and the transition is near critical. However, the free energy differences are small, so the molecular details become important for the stability of the ripple phases. X-ray and freeze-fracture electron microscopy studies have confirmed the existence of two types of ripples. One has an asymmetric sawtooth profile with alternating thin and thick arms and a ripple repeat distance of 13 to 15 nm. The second one has a symmetric, sinusoidal profile with a repeat distance of 26 to 30 nm. The thermal history of the membrane plays a key role in regulating the relative proportion of the two ripple phases. The asymmetric ripple phase forms at the pretransition temperature upon heating from the L'_β phase, while both the asymmetric and the symmetric phase form at the main phase transition temperature upon cooling from the liquid phase. The free energies of the two ripple phases are believed to be very similar, and the exact proportion of asymmetric and symmetric phases depends critically on the detailed cooling protocol [14]. The symmetric phase has been reported to be metastable and will eventually convert to the asymmetric (stable) phase at low temperature [14].

* Corresponding author.
E-mail address: adam@memphys.sdu.dk (A.C. Simonsen).
[1] Now at: Odense University Hospital, Radiophysical Laboratory, Denmark.
[2] Now at: Institute of Chemical Engineering, Biotechnology and Environmental Technology, University of Southern Denmark.

0005-2736/$ – see front matter © 2011 Elsevier B.V. All rights reserved.
doi:10.1016/j.bbamem.2011.08.023

Insight into the molecular structure of the ripple phases has been obtained from molecular dynamics [27,28] and Monte Carlo simulations [29]. In an atomistic model, de Vries et al. [27] produced an asymmetric rippled structure when cooling a DPPC lipid bilayer from the liquid phase. The structure consists of two subdomains, where in one subdomain, the lipids are organized as a splayed solid, and in the other, the lipids are solid-like and fully interdigitated. In the concave region between the subdomains, the lipids are disordered. Lenz and Schmid [29] have produced symmetric and asymmetric ripples in lipid bilayers by Monte Carlo simulations of a coarse-grained molecular model. The asymmetric rippled structure found is very similar to that found by de Vries et al. except that the fully interdigitated subdomain is replaced by a narrow interdigitated line. In the symmetric rippled structure, the membrane maintains its bilayer arrangement, but the individual leaflets contain curved, ordered stripes, where the upper and lower monolayers are interlocked. The stripes end with conical regions of disordered lipids, and the membrane assumes an overall sinusoidal shape. The findings of fractions of disordered lipids in the ripple phases are supported by theoretical [10] and experimental work [30–31]. Lenz and Schmid suggest that the ripple formation is driven by the tendency of lipids with large head groups to exhibit a splay. This observation is supported by molecular dynamics simulations of membranes containing simple model lipids by Sun and Gezelter [28]. They constructed a phase diagram showing the existence of asymmetric and symmetric ripple phases as well as a flat bilayer as a function of the head group-molecular width ratio and the strength of the head group dipole moment. The diagram shows that the bilayer phase is governed almost entirely by the head-to-tail size ratio, while the strength of the lipid dipole controls the stability of the phase. Neder et al. have found by coarse grained simulations that under tension the ripple phase disappears and is replaced by a fully interdigitated phase [32]. Hydrostatic pressures up to 3000 atm have the opposite effect and can induce a transition from the fluid to the ripple phase as demonstrated by Mark et al. [33].

The presence of an adjoining solid support will generally suppress the formation of the ripple phase in membranes, depending on the strength of the solid–membrane interaction. In 1994, Mou et al. used vesicle fusion to produce single supported bilayers which displayed ripple phase formation upon the addition of Tris–buffer, as observed by AFM [34]. In a subsequent paper, the same lab presented ripple phase formation in asymmetric single supported bilayers prepared by Langmuir–Blodgett deposition and imaged under specific salt concentrations [35]. Symmetric single supported bilayers of phospholipids have not been reported to exhibit ripples when buffers besides Tris are used. Although suppressed in single supported bilayers, ripples have been found to persist in double supported bilayer systems [36–38] because the top bilayer is more weakly interacting with the support. When cooling DPPC from the liquid state into the ripple temperature range, both the symmetric and the asymmetric phases were found by AFM as determined from periodicity and amplitude measurements, and macro-ripples with twice the ripple repeat distance of the symmetric ripples were also observed [37]. Ripple formation and disappearance at the pretransition was studied, showing that single ripples can appear or disappear one at a time upon heating or cooling, respectively. Also, the melting behavior of two-component DMPC–DSPC systems was studied in great detail. For such systems close to the solidus line, an interconversion of the symmetric to the asymmetric phase was observed, and upon further heating the symmetric phase melted prior to the asymmetric phase. These findings support the notion that the asymmetric phase is the thermodynamically stable variant [37]. In the ripple phase/liquid phase coexistence region, straight-edged anisotropic domains were observed. It was found that ripple phase formation was directly responsible for the anisotropic nature of the domain pattern [36].

Parallel to the observation of rippled membranes, narrow stripe domains of 10–100 μm length have repeatedly been reported in GUVs of binary mixtures of PC-lipids [39–46]. A typical example is found in reference [44] showing a mesh of narrow linear domains in a membrane with equimolar DLPC and DPPC. At high temperatures, the bilayer is in the liquid phase, but at lowered temperatures, solid ordered lines appear on the vesicles. These grow as the temperature is further lowered. Such stripe domains are often found to have characteristic bending angles at approximately 60° and 120° [39,45], and they tend to form percolating networks that span the entire vesicle [39,40,42,45,46]. Some reports suggest that the phase state of the stripe shaped domains is the ripple phase [39,45] while others claim that they correspond to the L'_{β} phase [40]. So far, no concluding evidence exists which assigns a specific phase to such stripe domains.

In this work, we pursue an integrated characterization of the ripple phase and the stripe domains in binary membranes using Atomic Force Microscopy (AFM) and fluorescence microscopy. Our setup allows correlated imaging of the same sample region with both techniques. We focus on systems close to the liquidus line and investigate the domain formation process as the bilayer is cooled from the liquid phase into the coexistence region. Several mixtures have been investigated, but we focus on the results obtained for the binary mixture of equimolar DLPC and DPPC. We work with double supported membranes prepared using a spin-coating and hydration protocol which allows easy and reproducible preparation of stacked bilayers with a wide range of lipid compositions [47].

2. Materials and methods

2.1. Materials

1,2-dipalmitoyl-sn-glycero-3-phosphocholine (DPPC) and 1,2-dilauroyl-sn-glycero-3-phosphocholine (DLPC) were purchased from Avanti Polar Lipids and used without further purification. The membrane probe 1,1′-dioctadecyl-3,3,3′,3′-tetramethylindocarbocyanin perchlorate (DiI-C_{18}) was from Invitrogen. Sodium phosphate, dibasic (>99%) and sodium phosphate, monobasic (>99%) were from Sigma, while NaCl (>99.5%) was from Fluka. Methanol from Sigma and n-hexane from Fluka were HPLC grade quality, and ultra pure Milli-Q water (18.3 MΩ cm) was used in all steps involving water. Phosphate buffer (10 mM phosphate, 128 mM NaCl) was prepared at pH 7.0 by mixing the appropriate amounts of di- and monobasic sodium phosphate and has a ionic strength of 150 mM. Muscovite mica (75 mm × 25 mm × 200 μm sheets) was from Plano GmbH, Germany. Mica sheets of 10 mm × 10 mm were preglued onto round (0.17 mm, 24 mm) microscope coverslips using a transparent and biocompatible silicone glue (MED-6215, Nusil Technology, Santa Barbara, CA). Immediately prior to spincoating, the mica is cleaved with a knife, leaving a thin and transparent mica film on the coverslip.

2.2. Preparation of supported lipid bilayers

To prepare a dry spin-coated lipid film on mica, we used a stock solution of 10 mM lipid mixture containing 0.5% DiI-C_{18} in hexane/methanol (97:3 volume ratio). A droplet (30 μL) of this lipid stock solution was then applied to freshly cleaved mica and immediately thereafter spun on a Chemat Technology, KW-4A spin-coater at 3000 rpm for 40 s. The sample was then placed under vacuum in a desiccator for 10–15 h to ensure complete evaporation of solvents. To hydrate the dry spincoated film, the sample was moved to the fluid cell (BioCell, JPK Instruments, Berlin, Germany). Phosphate buffer was added and the immersed sample was heated to 55 °C for 1 h. The sample was then placed on the fluorescence microscope and flushed with 55 °C buffer using a pipette adjusted to 500 μL. By monitoring the response of the lipid film while washing, the removal of lipid layers was accurately controlled. After the washing procedure, the liquid volume was gently exchanged 5–10 times to remove

membranes in solution. Further details of the sample preparation can be found in [47].

2.2.1. Epi-fluorescence microscopy

A Nikon TE2000 inverted microscope with a 40× long working distance objective (Nikon, ELWD, Plan Fluor, NA = 0.6) was used for epi-fluorescence observations. Fluorescence excitation was done at 540 nm with a Xenon lamp (PolychromeV, Till Photonics GmbH, Gräfelfing, Germany) and a G-2A filter cube (Nikon) appropriate for the DiI probe was used for imaging. Images were recorded with a high-sensitivity em-CCD camera (Sensicam em, 1004×1002 pixels, PCO-imaging, Kelheim, Germany) and operated with TILLvisION software (Till Photonics GmbH). Epi-fluorescence images were analyzed with ImageJ (National Institute of Health, USA) and custom m-files written in MATLAB™.

2.2.2. AFM imaging

Atomic force microscopy was performed using a JPK Nanowizard AFM system (JPK Instruments AG) operated in contact mode. The AFM is mounted on the fluorescence microscope described above. Silicon nitride cantilevers of the triangular type (MSCT, D-lever, Veeco) were used, with a nominal spring constant of 0.03 N/m and a resonance frequency of 15 kHz. During scanning, the sample was located in the fluid cell (BioCell, JPK Instruments AG) also used for fluorescence imaging. AFM images were processed and analyzed using the scanning probe image processor (SPIP; Image Metrology, Hørsholm, Denmark). SPIP includes a module for Fourier analysis of AFM images.

2.3. Continuous cooling experiment

To observe domain nucleation and growth, samples were cooled continuously from high temperatures, where the lipid bilayer is in the liquid phase to low temperatures, where solid phase domains coexist with the liquid phase. Samples were cooled at approximately 1 °C/min from 50 °C to 20 °C, and the temperature was recorded with an accuracy of 0.1 °C using a thermal sensor placed in the liquid cell very close to the surface of the sample. Images were recorded manually at approximately 10 second intervals, and the corresponding temperature was noted.

3. Results

3.1. Thick and thin stripe domains grow in the distal bilayer

We first investigate the growth of domains in a double lipid bilayer (DLPC, DPPC 1:1) that is cooled from the liquid phase into the phase-coexistence region. The supported double bilayers prepared above the liquidus line are homogeneous and defect-free as visualized by epi-fluorescence microscopy in Fig. 1A. The region of the sample imaged in this figure contains two bilayers stacked on top of each other. We name the bilayer next to the mica and the one situated on top as the proximal and distal bilayers, respectively. The bright spots are small vesicles attached to the distal bilayer. These are difficult to remove by the washing without destroying the distal bilayer and they may occasionally become nucleation sites for domains in the distal bilayer.

As the sample is cooled, domains start to nucleate at positions scattered across the surface as seen in Fig. 1B. Solid domains are identified in the images as regions that exclude the fluorescent probe. Two populations of domains are identified in the images. The nucleation of the first population is initiated in the temperature range of 33.0 °C to 32.0 °C, while the nucleation of the second population is initiated in the temperature range from 32.0 °C to 31.6 °C. In Fig. 1B, domains belonging to the first population are larger than domains belonging to the second population. As the temperature is further lowered, domains belonging to the first population continue to grow in area and attain a flower like shape as seen in the insets in Fig. 1B. This development is entirely equivalent to that observed for domains in single supported bilayers of DOPC and DPPC as described previously [48] and we conclude that these domains belong to the proximal layer. The growth of domains in the second population (distal bilayer) is different as the domains switch from a dark state with a lower probe concentration to later extending with bright stripes having more probe than the surrounding liquid phase. This is illustrated in the inset of Fig. 1B and in Fig. 1C, it is seen that thin stripes extend from the edges of the dark domains. Stripe domains that do not start from a dark core are also observed.

In Fig. 1D (29.6 °C) we observe dark regions with smooth edges near the left border of the image. Since there are no stripe domains inside these regions they are interpreted as holes in the distal bilayer. It is well known that the area per lipid in solid phases is smaller than the area in the liquid phase [49]. Growth of solid domains will therefore result in a reduction of the total membrane area which for a supported bilayer will lead to hole formation.

The stripes extend further as the temperature is lowered, and exhibit bending and tip splitting with angles close to 60° as highlighted in the inset of Fig. 1D. Tip splitting occurs with a branching angle of ~60° and is only observed at the advancing end of the stripes and not from the sides of stripes. At 29.6 °C a class of thicker stripes appears to protrude from the domains. The growth velocity of these thick stripes is significantly lower than the growth velocity of the thin stripes. The growth of the thick stripes takes specific directions relative to other thick stripes in the same domain. In Section 3.5, we analyze the stripe angles and growth speeds quantitatively. At a temperature of 28.1 °C, many thin stripes have become so long that they have collided with other domains and the thin stripes form a percolating network. This is observed in Fig. 1E.

At a temperature of 22.2 °C (Fig. 1F) the thick stripes have extended notably, and now these domains also percolate the entire distal bilayer. The width of the thick stripes increases, such that their aspect ratio remains rather constant during the growth. When the front of stripes collides with other domains, distortion of both thick and thin stripes occurs and the straight lines and sharp bending angles are modified as in Fig. 1F. The emergence and growth of holes in the distal bilayer also contributes to the distortion of the stripe network. As previously suggested [48], the reduction in the molecular area as the lipids solidify creates tension in the bilayer. This tension is partly relieved by holes, but the inhomogeneous distribution of tension forces also distorts the stripe network. At 22.2 °C, much of the fluorescent probe in the distal bilayer is absorbed in the stripe domains. This makes it difficult to distinguish between holes and the liquid phase in the distal bilayer. At 22.2 °C, cooling was terminated, and the growth of the domains stopped.

3.2. Thick and thin stripes correspond to symmetric and asymmetric ripples

To examine the phase state of stripe domains we use AFM at regions selected by fluorescence microscopy. Fig. 2A–D shows fluorescence images of a region of the sample recorded at four different temperatures. In Fig. 2A, a thin stripe extends from the domain indicated by an arrow. As the temperature is lowered, the stripe grows until it collides with another domain as observed in Fig. 2D. The second domain consists of a central region from which five thick stripes extend. This domain does not have a dark region at the nucleation point.

Fig. 2E shows an AFM image of the region highlighted in Fig. 2D. The condensed regions are easily recognized as being higher (brighter) than the fluid regions. The shape of the domain region observed in the AFM image corresponds well to the shape of the domain observed in the fluorescence image. Small deviations may arise because the AFM image was obtained a few hours after the image in Fig. 2D.

Domains residing in the proximal bilayer are also observed in the left and top part of Fig. 2E. In double bilayer systems, these domains

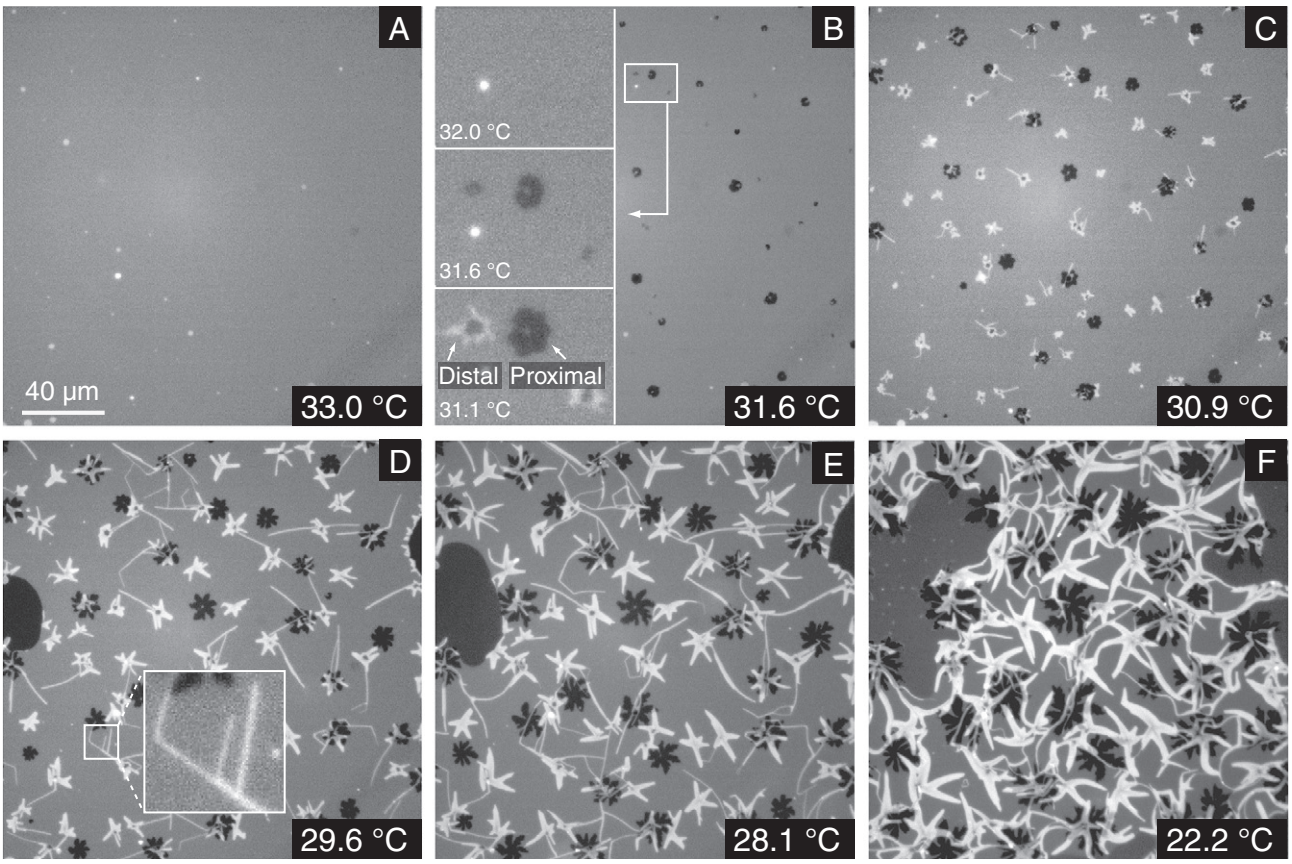

Fig. 1. Sequence of fluorescence images recorded during the cooling of a double membrane system with composition DLPC and DPPC (molar ratio 1:1). The temperature for each image is indicated. The entire system is initially in a homogeneous fluid state (A) and cooling leads to the nucleation and growth of condensed domains (B–F). The proximal membrane contains dark domains only, while the distal membrane also displays bright stripe-shaped domains. The distinction between domains in distal and proximal bilayers is pointed out in the inset of (B). Inset in (D) shows an example of tip splitting and bending in growing stripes.

are usually observed by AFM as imprints in the distal bilayer as previously found by Leidy et al. [36,37]. The line scan in Fig. 2E shows that the thick and thin stripes have different heights. The thin stripe is approximately 2 nm higher than the surrounding liquid regions, while the thick stripe is 5–6 nm higher than the liquid regions. The two square regions of the domain which are highlighted in Fig. 2E are further investigated in Fig. 2F and G.

The AFM image of the central region of the domain is shown in Fig. 2F and displays a surface with periodic corrugations. The line scan (blue line) indicates that the corrugations have a period of approximately 30 nm, thus agreeing well with the ripple repeat distance of the symmetric ripple phase. The ripple orientation is constant over extended areas, but changes direction at specific straight line defects. At least five regions with constant ripple orientation are identified in the image. The orientation of the ripples in these regions is highlighted by thin white lines in the image. When compared to the corresponding fluorescence images in Fig. 2A–D, we notice that the growth directions of the stripes extending from the domain are parallel to the ripple orientations. We also note the presence of a central point defect in the center of Fig. 2F corresponding approximately to the location of the nucleation point.

In Fig. 2G, an AFM deflection mode image of the region where the thin stripe touches the domain is shown. In this case two types of corrugations are observed. The line scan in the figure is based on data from the corresponding AFM height mode image. It indicates that the corrugations have a period of approximately 13 nm in the region of the thin stripe. This corresponds very well to the ripple repeat distance of the asymmetric ripple phase.

A 2 dimensional Fourier transform (power spectrum) of the deflection mode image in 2G is shown in Fig. 2H. From the spots in the image we determine the wave vectors $\mathbf{k}_1$ and $\mathbf{k}_2$ associated with the two types of ripples in the image. It is seen that $\mathbf{k}_1$ is oriented perpendicular to the ripple orientation in the thick stripe, while $\mathbf{k}_2$ is oriented perpendicular to the ripple orientation in the thin stripe. The ripple periods are conveniently obtained from the wave vectors in the SPIP software as $\lambda = |\mathbf{k}|^{-1}$ [50]. We find that $\lambda_1 = |\mathbf{k}_1|^{-1} = 27.4 \pm 0.6$ nm and $\lambda_2 = |\mathbf{k}_2|^{-1} = 13.5 \pm 0.2$ nm. From these measurements we conclude that the phase state of the thick and thin stripes is the symmetric ripple phase and asymmetric ripple phase, respectively. Furthermore, we have shown that the ripples are oriented parallel to the growth direction of the stripes.

3.3. The dark domain core is in the L'_β phase

To examine the nature of the dark domain cores, we again combine AFM and fluorescence. Fig. 3A shows an AFM deflection image of the core region of the domain corresponding to the fluorescence image of Fig. 3B. The average ripple repeat distance in the region as determined from the Fourier transform in Fig. 3F, is 29.5 ± 1 nm. These ripples are therefore of the symmetric type. The pixel resolution (4 MP) in Fig. 3A is not sufficient to resolve the asymmetric ripples of the thin stripe. Although the doubling of the small, unidentified spots in the AFM recording indicates a double AFM tip, this does not affect the ripple repeat distance because the height variations in ripples are smaller than the double tip.

In Fig. 3C, the AFM height mode image of the center of the domain is shown. From the image we identify three different heights: The tallest is the border region corresponding to the symmetric ripple phase, the lowest region is located at the center of the domain, while a region of intermediate height is found between these two. The region

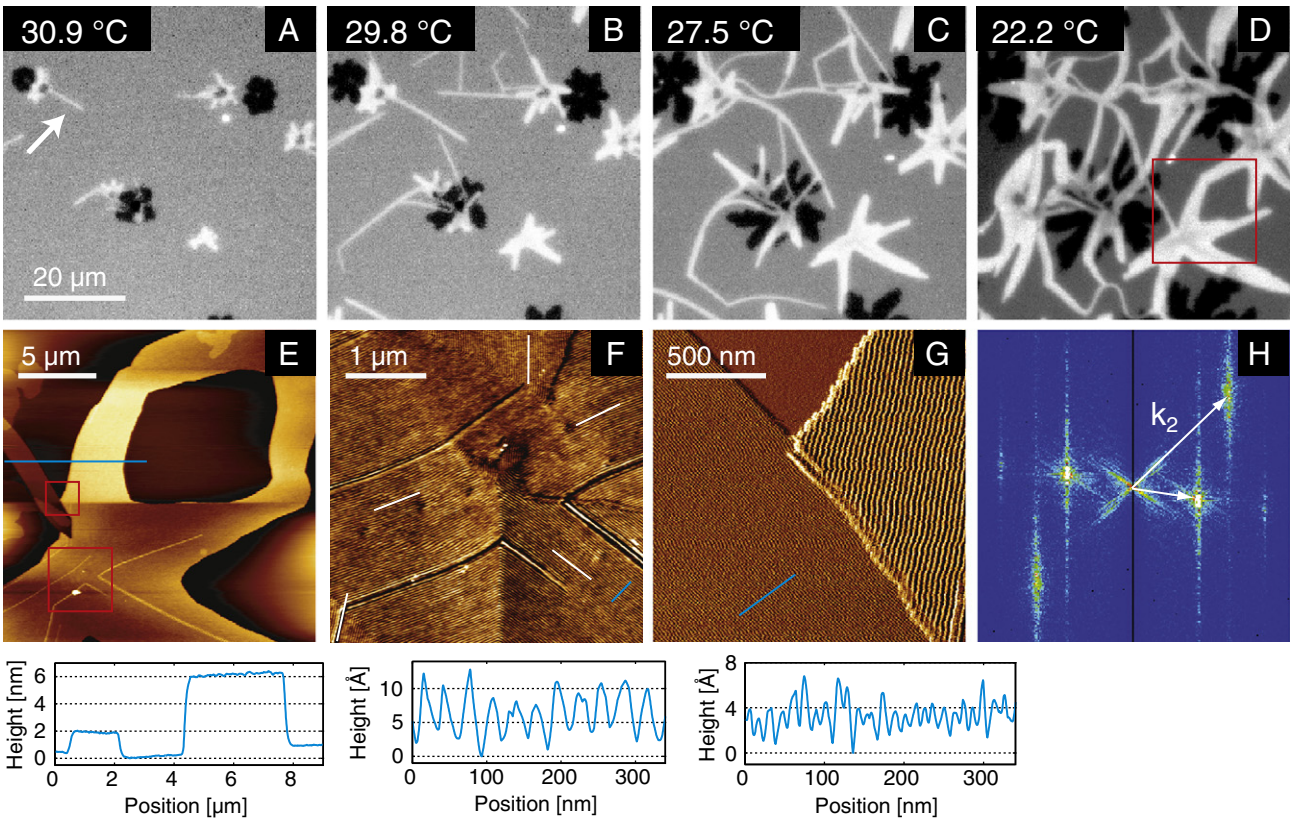

Fig. 2. Topography of stripe domains. Fluorescence sequence (A–D) focusing on the growth and collision between a thin stripe domain (arrow) and a star-shaped domain with five thick stripes. AFM topography image (E) of the square region highlighted in (D). AFM topography image (F) of the central region of the domain as indicated in (E). The period of the corrugations as observed in the line scan corresponds to the period of the symmetric ripple phase. The five prominent ripple directions are indicated in the image (white lines) which are parallel to the growth directions of five thick stripes of the domain. AFM deflection mode image (G) of the region where the thin stripe touches the domain, as indicated in (E). The period of the corrugations observed in the thin stripe (line scan) corresponds to the period of the asymmetric ripple phase. Fourier transform (H) of the image in (G). From the vectors $\mathbf{k}_1$ and $\mathbf{k}_2$ the ripple repeat distances and ripple directions are obtained.

of intermediate height is the asymmetric ripple phase because this region follows the path of the thin stripe as observed in Fig. 3B. From Fig. 3C we also obtain that the symmetric ripples are 4 nm higher than the asymmetric ripples. This agrees fully with the line scan shown in Fig. 2E. The height difference of 4 nm also agrees with literature values for the peak-to-peak thicknesses of symmetric ripple phase, 10.5 nm (for DPPC [51]), and asymmetric ripple phase, 6.5 nm (for DMPC [51] — the thickness of asymmetric ripple phase for DPPC has not been reported in literature). Since DiI-C_{18} is excluded from the L'_β phase [48] we conclude that the probe-excluding region found at the nucleation center consists of the L'_β phase. The three different phases identified around the domain core are marked on the schematic illustration in Fig. 3E.

3.4. Templated growth of thick stripes on thin stripes

During growth of the ripple domains, we observe that thick stripes increase in both length and width. By inspection of the fluorescence images in Fig. 1D and E, we can see that some of the thin stripes apparently increase in width during growth, while another group retains a rather constant width. To understand this observation, we investigate with AFM a region where thin stripes are growing in width during the cooling process. Fig. 4A shows a fluorescence image of the double bilayer structure where several thin stripes exhibit a change of width at locations indicated by the arrows. In Fig. 4B–D, we observe how the wide part of the thin stripes extends along the body of stripe, while the thin regions of the stripes retain a constant width during the temperature reduction.

Fig. 4E shows an AFM image of a part of the region under investigation after the cooling process is terminated. Three different heights are observed in the image, which correspond to the liquid, asymmetric, and symmetric ripple phases. The image does not have enough pixels to resolve the ripple structure, but the phases are easily identified from the height profiles. We notice that stripes consisting of the asymmetric ripple phase do not change width at any location in the image. However, we observe that stripes composed of the symmetric ripple phase are located immediately next to the thin stripes in certain regions. By detailed comparison between the AFM (Fig. 4E) image and the fluorescence images in Fig. 4A–D, we observe that the locations where the thin stripes change width correspond to these regions. These findings show that the thin stripes do not change width during the domain growth. Instead, they function as templates for the growth of the symmetric ripple phase. We notice a characteristic curved growth front of the symmetric ripple domains as indicated by the arrows in Fig. 4E. This curvature appears to be a general feature of the growth front of thick stripes.

The observations above indicate that asymmetric ripple domains grow almost exclusively in length and not in width. When the growth front of thin stripes encounter obstacles (other domains), this phase apparently ceases to grow further. Because the thin stripes only split at the growth front, hardly any new thin stripes are generated in the later stages of the cooling process. In fact, the thin stripes are mostly generated immediately after the nucleation process and only observed to grow from domains containing a dark nucleation center of the L'_β phase. Due to this correlation between the formation of L'_β domains and asymmetric ripples it is possible that the density of L'_β

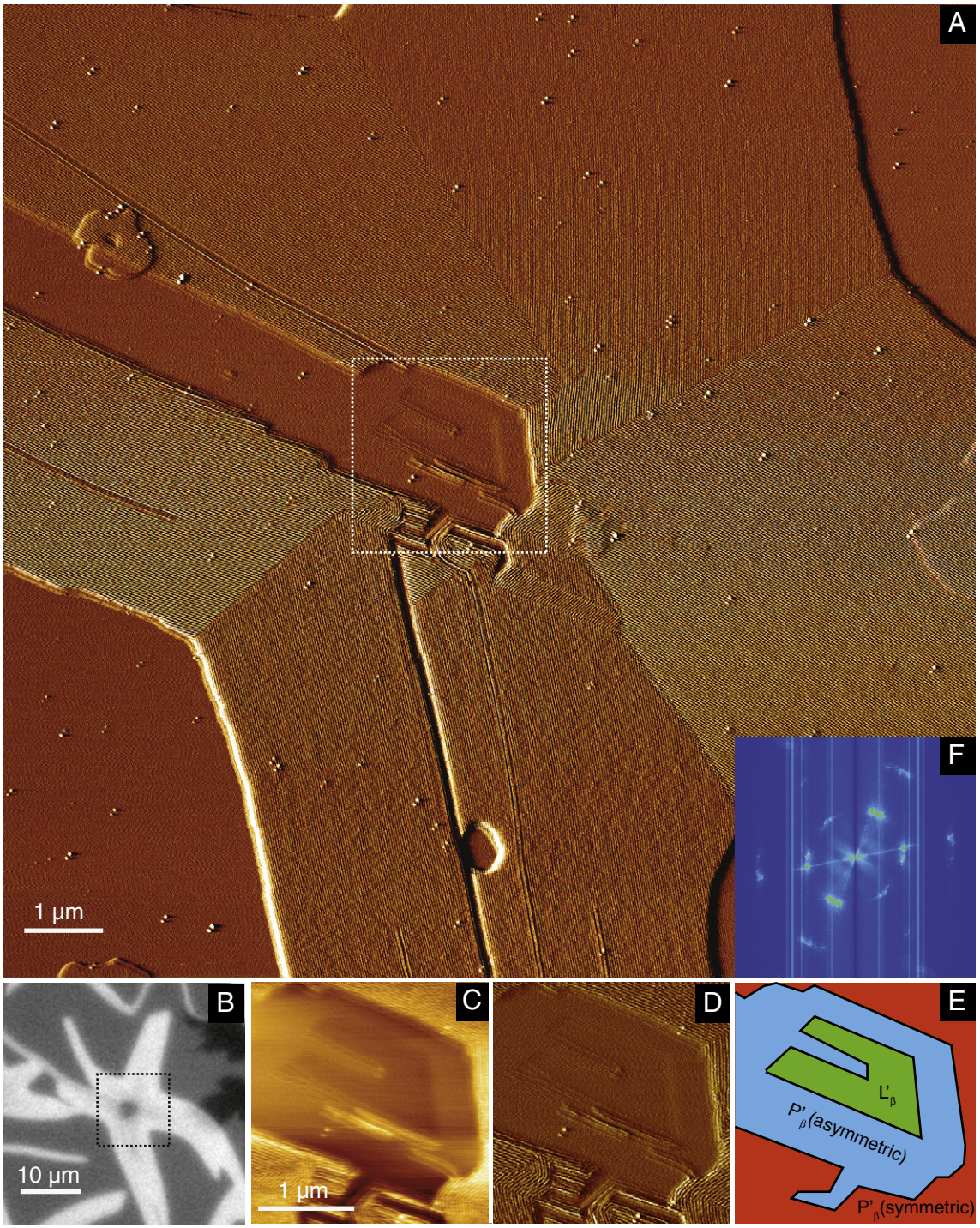

Fig. 3. AFM deflection image (A) of the central region of the domain as shown in the fluorescence image (at 22.2 °C) of (B). Height (C) and deflection (D) AFM images of the region surrounding the nucleation point as indicated by the square in (A). Schematic illustration (E) of the three phases, L'_β = green, P'_β(asymmetric) = blue, P'_β(symmetric) = red, which were identified around the nucleation point (see text). 2D Fourier transform (F) of the AFM image in panel A.

nucleation points eventually controls the ratio of asymmetric to symmetric ripple phases in the phase-coexistence region. However, this remains to be confirmed quantitatively.

3.5. Angles and growth velocities of stripe domains

At temperatures slightly below the nucleation temperature, thin stripes have not collided with other domains. The shape of these domains has also not been distorted by lateral tension in the membrane. We use this regime to quantify the intrinsic bending angles of thin stripes. This is done by manual measurements of 30 bending angles in an image recorded at 29.6 °C. Fig. 5A shows the histogram of these bend angles. One narrow population of bending angles exists with a mean value of 115.3°. It is interesting to note that on the occasions where a stripe bends more than once, the bending is always to the same side. In most cases, the stripes bend to the right hand side with respect to the growth direction, but bending to the left hand side is also observed. As discussed in Section 3.1, tip splitting can

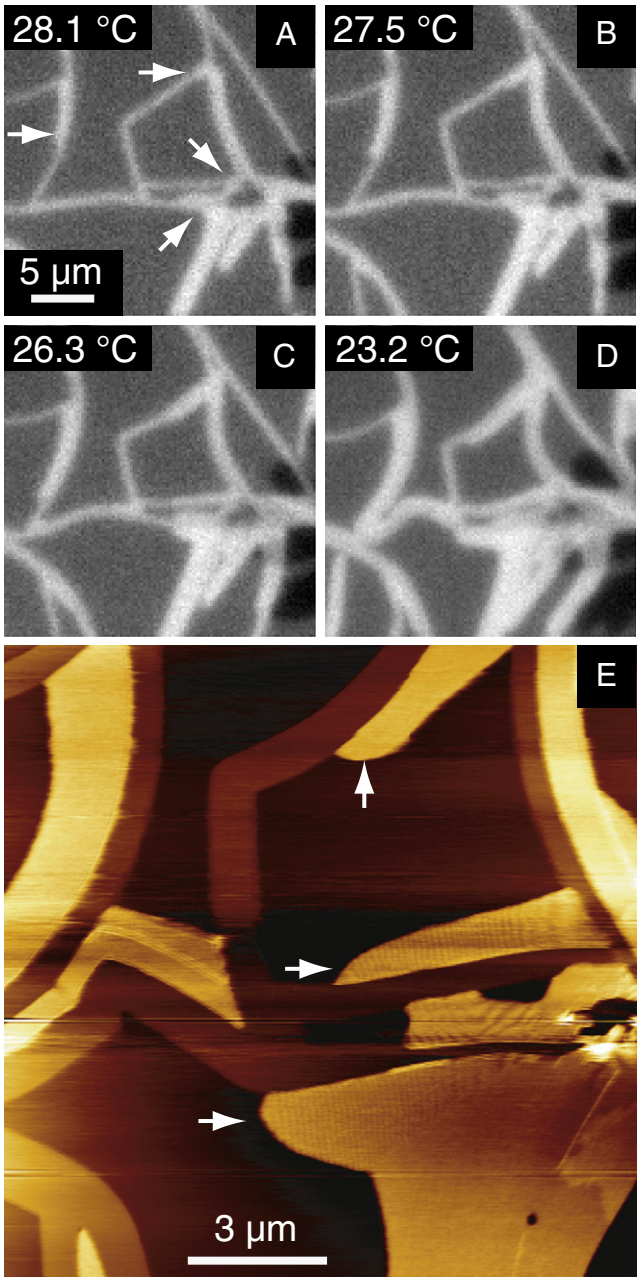

Fig. 4. Templated growth of the symmetric ripple phase along the sides of asymmetric ripple phase domains. Fluorescence image (A) with several initially thin stripe domains that, upon cooling, increase in width at the positions indicated by the arrows. The increase in width of these domains is shown in (B–D). Corresponding AFM image (E) showing how the stripe domains are composed of a mixture of symmetric and asymmetric ripples.

also be observed. For single stripes, branching always happens to the same side of the stripe and to the same side as any previous or subsequent bending. We suggest that the preference for bending and tip splitting to one particular side is a consequence of the asymmetric shape of the ripple waves, possibly in combination with the presence of the proximal bilayer.

As noted in Section 3.1, the thick stripes appear to have specific directions relative to the other thick stripes in the same domain. To analyze this observation in detail, the intersection angles between thick stripes originating from the same nucleus were measured manually for an image recorded at 30.3 °C. Fig. 5B (inset) illustrates the location of an intersection angle. A total of 139 angles in 28 domains were measured manually as shown in the histogram of Fig. 5B. The intersection angles cluster around 0°, 60° and 120°. A trimodal Gaussian fit is also shown where the peaks of the fit are centered at 3°, 59° and 119°. The characteristic bending angles and intersection angles found in domains in the distal bilayer reflect the underlying six fold order of the condensed membrane phases.

The growth velocity of the stripes was quantified using an automated image analysis algorithm. Fig. 5C shows a plot of the extension of a thin and a thick stripe as a function of time in the temperature range between 30.9 °C and 29.2 °C. Of course, the growth velocities are only with reference to a specific cooling ramp, but relative differences between thin and thick stripes are expected to be universal. The extension length of stripes generally increases linearly in time for all investigated stripes. The slope of the two fits shown in Fig. 5C is 115 nm/s and 42 nm/s for the thin and the thick stripe, respectively. A histogram of growth velocities for 35 different stripes is shown in Fig. 5D. The two populations correspond to thin and the thick stripes, respectively. The thick stripes have a mean growth velocity of 36 nm/s, while the mean growth velocity of the thin stripes is 133 nm/s. Thus, the thin asymmetric ripple phase grows more than three times as long as the symmetric ripple phase over a given time.

4. Discussion

Spin-coating has previously been used for the preparation of supported bilayers of a single component [52] and ternary mixtures of lipids [53,54]. The advantages of supported bilayers compared to GUVs are the possibility to study rapid processes by time-lapse microscopy over extended periods of time and the facilitation of advanced image analysis by the planar geometry [52–55]. Spin-coating can be used favorably to produce double bilayers where the second bilayer preserves most properties of free standing membranes. The stripe-shaped domains presented here are indeed similar to domains observed in GUVs of the same mixture [39,42–45]. Also other binary mixtures such as DOPC/DPPC [40,41], POPC/DPPC [46], DLPC/DSPC and DMPC/DSPC [39,43], DMPC/DPPC and DPPC/DSPC [39] display stripe-shaped domains in the solid ordered/liquid disordered phase coexistence region. These common observations call for an explanation of the nature of the stripes. Previously, it has been suggested that the phase state of stripes observed in GUVs is the ripple phase [39,45]. In the work presented here we have substantiated this hypothesis by direct experimental evidence. To our knowledge, co-localized AFM and fluorescence microscopy has not been used to study ripple phase structures. The combination of the two techniques gives significant new insight into the correlation between membrane domain morphology and phase state.

Finding similar domain shapes and sizes in supported double bilayers and free standing bilayers is a clear indication of the versatility of the spin-coating technique. We can furthermore compare the location of the liquidus line in the phase diagram of the mixture to the nucleation point temperature observed for the supported bilayers. Seeger et al. have presented a phase diagram of the DLPC/DPPC mixture [56] based on heat capacity profiles. The liquidus temperature of the equimolar mixture extracted from the phase diagram is 32–33 °C. We have observed the nucleation of solid ordered domains in the proximal bilayer at 33 °C and in the distal bilayer at 32 °C. These measurements show that ensemble physical chemical properties of lipid systems can be studied at the level of a single membrane prepared by spin coating. The slightly higher nucleation temperature of the proximal bilayer compared to the distal bilayer probably arises from the interaction with the support. However, this interaction is minimal in our system, because the charges in the bilayer and the support have been screened by counter ions from the high levels of salt as reported by Keller et al. [53,57].

Literature gives somewhat conflicting information on the partitioning of DiI-C_{18} into various membrane phases [58]. The probe was

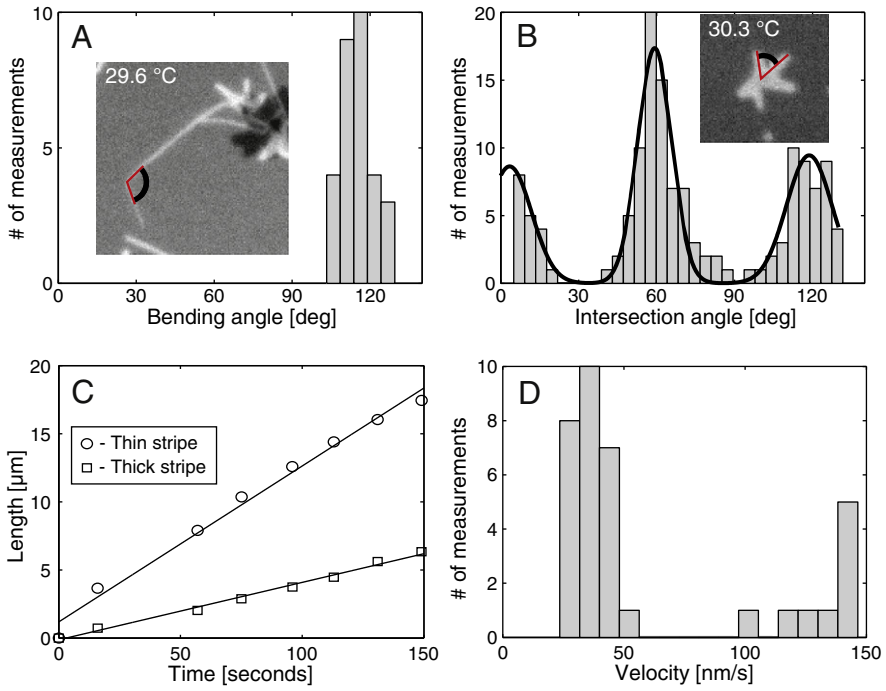

Fig. 5. Distribution of bending angles for single stripe domains that display kinks (A). Intersection angles of stripe domains that originate from the same nucleation point (B). Both (A) and (B) where measured at temperatures where the forces between domains have not distorted the angles. Quantification of the growth velocity of the stripe-shaped domains (C–D). Plot of the extension length of a thin and a thick stripe (C). The extension length is linear in time in this regime. The slope of the length versus time curves yields the growth velocity which is plotted as a histogram in (D) for 35 stripes. Two populations are evident: One for slower growing thick stripes and another for faster growing thin stripes.

reported to partition preferentially into the solid ordered phases over the liquid disordered phase [59]. This has been confirmed by confocal fluorescence images of GUVs composed of DOPC/DPPC [41] and DLPC/DPPC [40]. In these papers, the solid ordered domains were stripe-shaped. However, in binary mixtures composed of POPC and ceramide, DiI-C_{18} is excluded from the solid phase [60]. This is in line with the results presented here, where we find low partitioning into the L'_β phase compared to the liquid phase in supported bilayers composed of DLPC and DPPC. Our finding that the stripe shaped domains are indeed composed of the ripple phase clarifies these issues. According to our observations, DiI-C_{18} partitions preferentially into the ripple phases over the liquid phase, but preferentially into the liquid phase over the L'_β phase. The reason for this difference in the partitioning properties of DiI-C_{18} is not obvious. The long saturated chains of the probe prefer an ordered environment, which both the ripple phases and the L'_β phase possess. However, the large fluorescent head group of the molecule may fit poorly into the flat, tilted geometry of the L'_β phase, while the corrugated surface of the ripple phases could provide the required space needed in the splayed regions of the ripple ridge.

Our results suggest that when cooling the binary mixture from the liquid phase into the solid ordered/liquid disordered phase-coexistence region, domains of the L'_β phase may nucleate and function as templates for the growth of the ripple phases. In these cases, we observe the coexistence of four different phases over a range of temperatures: L'_β, asymmetric ripple, symmetric ripple, and the liquid phase. The symmetric ripple phase is most likely metastable, and when applying Gibbs' phase rule, this phase should not be counted in. For constant pressure, the rule is reduced to

$$F = C + 1 - P, \tag{1}$$

where F is the number of degrees of freedom of the system, C is the number of components, and P is the number of coexisting phases. With two components and three coexisting phases, there should be no degrees of freedoms of the system, and a change in temperature should lead to a reduction of the number of coexisting phases. This is not observed in our system, which means that one phase should be metastable. Gordon et al. [39] have suggested a binary phase diagram, where a metastable $L_\alpha + L'_\beta$ coexistence region overlaps with the equilibrium $L_\alpha + P'_\beta$ coexistence region. We briefly describe their hypothesis and Fig. 6 shows an adapted version of their phase diagram [8,39]. Equilibrium phase boundaries are given by solid lines, while dashed lines outline the metastable $L_\alpha + L'_\beta$ coexistence region. During slow cooling, domains nucleate at point 1 in the diagram. Here the bilayer can only separate into $L_\alpha + P'_\beta$ coexistence. But a faster cooling could take the system into the metastable solid ordered/liquid disordered coexistence region. For domains nucleating at point 2 in the diagram, the system may partially lower its free energy first by separating into coexisting $L_\alpha + L'_\beta$ regions with compositions given by the points A* and B*, before reaching equilibrium by separating into $L_\alpha + P'_\beta$ phases with compositions given by the points A and B.

Coexisting stripe- and patch-shaped domains have been observed in GUVs composed of DOPC/DPPC and DLPC/DPPC at different molecular ratios by Li and Cheng [40]. These authors found that the patch-shaped domains functioned as nucleation sites for the growth of stripe-shaped domains during cooling. Nucleation of L'_β domains may be facilitated by a lower L_α/L'_β interfacial tension compared to the L_α/P'_β interfacial tension. Furthermore, the L'_β phase may function as a template for the growth of the P'_β phase if the L'_β/P'_β interfacial tension is lower than the L_α/P'_β interfacial tension. All of the above mentioned interfacial tensions are most likely anisotropic, and will depend on the orientation of the tilted lipids with respect to the domain boundary. It is interesting that those ripples of the symmetric ripple phase that are close to the interface between the asymmetric and symmetric phase in Fig. 3D are parallel to the interface. As mentioned, Fig. 3D does not resolve the ripple orientation of the asymmetric ripple phase, but assuming that the ripple orientation of the asymmetric ripple phase is parallel to the ripples of the symmetric ripple phase, the asymmetric ripples will be oriented parallel to the L'_β/P'_β interface. It is known that in the asymmetric ripple phase, the lipids have a net tilt orthogonal to the ripples [61]. Furthermore, we have previously shown that lipids in the L'_β phase display a complex

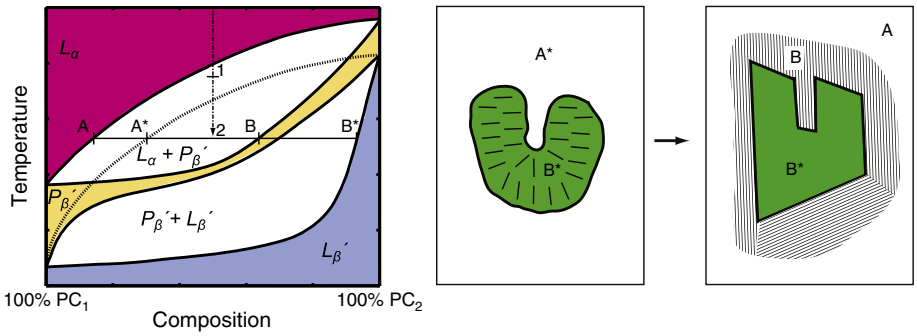

Fig. 6. Generic temperature–composition phase diagram of a binary phospholipid membrane adapted from Gordon et al. [40] (left). The diagram shows metastable $L_\alpha + L'_\beta$ coexistence region overlaps with the equilibrium $L_\alpha + P'_\beta$ coexistence region. Equilibrium phase boundaries are given by the solid lines, while the dashed line outlines the metastable $L_\alpha + L'_\beta$ coexistence region. Such a diagram could explain the formation of L'_β phase at the nucleation of the domains. Schematic illustration of a possible connection between orientational texture in the initial green gel L'_β domain (middle) and the orientation of the ripples that form later around this nucleation core (right). Symbols A, A*, B, and B* refer to local membrane compositions (stoichiometries) as provided in the phase diagram.

orientational texture in supported lipid bilayers [62]. In Fig. 3, we also note that the L'_β phase region of the domain has a characteristic horseshoe shape, not unlike the cardioid-shaped domains reported in some monolayer domains [63]. If the orientational texture of the horseshoe L'_β domains is as indicated in Fig. 6 it is not unlikely that the lipid tilt in the L'_β phase region of the domain in Fig. 3 is oriented orthogonal to the L'_β/P'_β interface. This would indeed indicate a reduced L'_β/P'_β interfacial tension, because the lipids would be tilted in the same direction on both sides of the interface.

The detailed processes going on at the border of the L'_β domain has importance for the generation of the asymmetric ripples. As mentioned in Section 3.4, the formation of the asymmetric ripple phase is only observed at domains containing a nucleation center consisting of the L'_β phase. Because the asymmetric ripple phase does not grow perpendicular to the ripples, the density of domains with a L'_β nucleation center controls the final ratio of asymmetric to symmetric ripple phase. In relation to these findings, it is interesting to note that scattering experiments suggest that it is the exact cooling procedure that determines this ratio [14]. Fast cooling leads to a high ratio, while slower cooling leads to a low ratio [13]. We have not performed experiments with different cooling rates for double supported bilayers, but our previous results for single supported bilayers of DOPC and DPPC suggest that fast cooling rates lead to a high nucleation density, while slow cooling rates lead to at low nucleation density [48]. Furthermore, the fast cooling rates also take the system into the metastable $L_\alpha + L'_\beta$ coexistence region before domains nucleate. Our findings are thus in line with the scattering data and could explain the ratios described earlier.

The anisotropic nature of the interfacial tension is most likely responsible for the formation of the stripe-shaped domains. What controls the thickness of the stripes is presently not known. Since it seems that they do not grow in width during cooling, we suggest that processes occurring at the domain nucleation site are responsible. It is likely that the size of the nucleation center, which consists of the L'_β phase, modulates this width. Future experiments will have to clarify these issues. However, the widths we measure are in the range of 1–2 μm, which matches those found in many GUVs.

One of the most surprising findings in this work was the very high growth velocity of the thin, stripe-shaped domains. We have shown that a very small, externally imposed change of the system (in our case a temperature change of $\Delta T < 1$ °C) can trigger the formation of structures that are several μm long in just a few seconds. It is interesting that this type of domain growth was indirectly observed by Winchil et al. in 1989 [64]. These authors used fluorescence recovery after photobleaching (FRAP) to demonstrate that a small fraction of a condensed membrane phase could disconnect diffusion in the remaining liquid phase. Based on this, they concluded that the domains must grow in a dendritic form. This is in agreement with the percolating networks we observe, which will essentially confine fluid phase diffusion to the domains that have been segmented by the stripes.

It is presently unclear which influence the ripple formation propensity of membrane lipids have in biological cells. However, if the ripple phase exists in natural membranes, the ability of the lipids to grow into a solid network very rapidly by using only a small fraction of the lipids to do so could be very useful to rigidify and compartmentalize the membrane.

Acknowledgements

The Danish National Research Foundation is gratefully acknowledged for support via a grant to MEMPHYS-Center for Biomembrane Physics.

References

[1] L.A. Bagatolli, J.H. Ipsen, A.C. Simonsen, O.G. Mouritsen, An outlook on organization of lipids in membranes: searching for a realistic connection with the organization of biological membranes, Prog. Lipid Res. 49 (4) (2010) 378–389.
[2] G. Pabst, S. Danner, S. Karmakar, G. Deutsch, V.A. Raghunathan, On the propensity of phosphatidylglycerols to form interdigitated phases, Biophys. J. 93 (2) (2007) 513–525.
[3] H.W. Meyer, H. Bunjes, A.S. Ulrich, Morphological transitions of brain sphingomyelin are determined by the hydration protocol: ripples re-arrange in plane, and sponge-like networks disintegrate into small vesicles, Chem. Phys. Lipids 99 (2) (1999) 111–123.
[4] P.H. Ververgaert, P.F. Elbers, A.J. Luitingh, H.J. van den Berg, Surface patterns in freeze-fractured liposomes, Cytobiologie 6 (1) (1972) 86–96.
[5] A.J. Verkleij, P.H. Ververgaert, L.L. van Deenen, P.F. Elbers, Phase-transitions of phospholipid bilayers and membranes of Acholeplasma-laidlawii B visualized by freeze fracturing electron-microscopy, Biochim. Biophys. Acta 288 (2) (1972) 326–332.
[6] A. Tardieu, V. Luzzati, F.C. Reman, Structure and polymorphism of hydrocarbon chains of lipids — study of lecithin–water phases, J. Mol. Biol. 75 (4) (1973) 711–733.
[7] H.W. Meyer, Pretransition-ripples in bilayers of dipalmitoylphosphatidylcholine: undulation or periodic segments? A freeze-fracture study, Biochim. Biophys. Acta, Lipids Lipid Metab. 1302 (2) (1996) 138–144.
[8] E.J. Luna, H.M. McConnell, Multiple phase-equilibria in binary-mixtures of phospholipids, Biochim. Biophys. Acta 509 (3) (1978) 462–473.
[9] J.A.N. Zasadzinski, J. Schneir, J. Gurley, V. Elings, P.K. Hansma, Scanning tunneling microscopy of freeze-fracture replicas of biomembranes, Science 239 (4843) (1988) 1013–1015.
[10] W.J. Sun, S. TristramNagle, R.M. Suter, J.F. Nagle, Structure of the ripple phase in lecithin bilayers, Proc. Natl. Acad. Sci. 93 (14) (1996) 7008–7012.
[11] B.G. Tenchov, H. Yao, I. Hatta, Time-resolved X-ray diffraction and calorimetric studies at low scan rates: I. Fully hydrated dipalmitoylphosphatidylcholine (DPPC) and DPPC/water/ethanol phases, Biophys. J. 56 (4) (1989) 757–768.
[12] D.C. Wack, W.W. Webb, Synchrotron X-ray study of the modulated lamellar phase p-beta′ in the lecithin–water system, Phys. Rev. A 40 (5) (1989) 2712–2730.

[13] S. Matuoka, H. Yao, S. Kato, I. Hatta, Condition for the appearance of the metastable p-beta′ phase in fully hydrated phosphatidylcholines as studies by small-angle X-ray-diffraction, Biophys. J. 64 (5) (1993) 1456–1460.
[14] J. Katsaras, S. Tristram-Nagle, Y. Liu, R.L. Headrick, E. Fontes, P.C. Mason, J.F. Nagle, Clarification of the ripple phase of lecithin bilayers using fully hydrated, aligned samples, Phys. Rev. E 61 (5) (2000) 5668–5677.
[15] M. Rappolt, G. Rapp, Structure of the stable and metastable ripple phase of dipalmitoylphosphatidylcholin, Eur. Biophys. J. 24 (6) (1996) 381–386.
[16] K. Mortensen, W. Pfeiffer, E. Sackmann, W. Knoll, Structural-properties of a phosphatidylcholine-cholesterol system as studied by small-angle neutron-scattering — Ripple structure and phase-diagram, Biochim. Biophys. Acta 945 (2) (1988) 221–245.
[17] P.W. Westerman, M.J. Vaz, L.M. Strenk, J.W. Doane, Phase-transitions in phosphatidylcholine multibilayers, Proc. Natl. Acad. Sci., Biol. Sci. 79 (9) (1982) 2890–2894.
[18] K. Tsuchida, I. Hatta, Electron-spin-resonance studies on the ripple phase in multilamellar phospholipid-bilayers, Biochim. Biophys. Acta 945 (1) (1988) 73–80.
[19] T. Heimburg, A model for the lipid pretransition: coupling of ripple formation with the chain-melting transition, Biophys. J. 78 (3) (2000) 1154–1165.
[20] P.A. Pearce, H.L. Scott, Statistical-mechanics of the ripple phase in lipid bilayers, J. Chem. Phys. 77 (2) (1982) 951–958.
[21] T.C. Lubensky, F.C. Mackintosh, Theory of ripple phases of lipid bilayers, Phys. Rev. Lett. 71 (10) (1993) 1565–1568.
[22] J.M. Carlson, J.P. Sethna, Theory of the ripple phase in hydrated phospholipid-bilayers, Phys. Rev. A 36 (7) (1987) 3359–3374.
[23] M. Marder, H.L. Frisch, J.S. Langer, H.M. McConnell, Theory of the intermediate rippled phase of phospholipid-bilayers, Proc. Natl. Acad. Sci., Phys. Sci. 81 (20) (1984) 6559–6561.
[24] S. Doniach, Thermodynamic model for the monoclinic (ripple) phase of hydrated phospholipid-bilayers, J. Chem. Phys. 70 (10) (1979) 4587–4596.
[25] P.L. Hansen, L. Miao, J.H. Ipsen, Fluid lipid bilayers: intermonolayer coupling and its thermodynamic manifestations, Phys. Rev. E 58 (2) (1998) 2311–2324.
[26] L. Miao, P. Hansen, J. Ipsen, Fluid lipid-bilayer membranes: some basic physical mechanisms for lateral self-organization, Les Houches Proceedings on Dynamical Networks in Physics and Biology, Springer-Verlag, Berlin, 1998, pp. 237–248.
[27] A.H. de Vries, S. Yefimov, A.E. Mark, S.J. Marrink, Molecular structure of the lecithin ripple phase, Proc. Natl. Acad. Sci. 102 (15) (2005) 5392–5396.
[28] X.Q. Sun, J.D. Gezelter, Dipolar ordering in the ripple phases of molecular-scale models of lipid membranes, J. Phys. Chem. B 112 (7) (2008) 1968–1975.
[29] O. Lenz, F. Schmid, Structure of symmetric and asymmetric "ripple" phases in lipid bilayers, Phys. Rev. Lett. 98 (5) (2007) 058104.
[30] M.B. Schneider, W.K. Chan, W.W. Webb, Fast diffusion along defects and corrugations in phospholipid p-beta′ liquid-crystals, Biophys. J. 43 (2) (1983) 157–165.
[31] K.A. Riske, R.P. Barroso, C.C. Vequi-Suplicy, R. Germano, V.B. Henriques, M.T. Lamy, Lipid bilayer pre-transition as the beginning of the melting process, Biochim. Biophys. Acta, Biomembranes 1788 (5) (2009) 954–963.
[32] J. Neder, B. West, P. Nielaba, F. Schmid, Coarse-grained simulations of membranes under tension, J. Chem. Phys. 132 (11) (2010) 115101.
[33] R. Chen, D. Poger, A.E. Mark, Effect of high pressure on fully hydrated DPPC and POPC bilayers, J. Phys. Chem. B 115 (5) (2011) 1038–1044.
[34] J.X. Mou, J. Yang, Z.F. Shao, Tris(hydroxymethyl)aminomethane (C4H11NO3) induced a ripple phase in supported unilamellar phospholipid-bilayers, Biochemistry 33 (15) (1994) 4439–4443.
[35] D.M. Czajkowsky, C. Huang, Z.F. Shao, Ripple phase in asymmetric unilamellar bilayers with saturated and unsaturated phospholipids, Biochemistry 34 (39) (1995) 12501–12505.
[36] C. Leidy, T. Kaasgaard, J.H. Crowe, O.G. Mouritsen, K. Jorgensen, Ripples and the formation of anisotropic lipid domains: imaging two-component double bilayers by atomic force microscopy, Biophys. J. 83 (5) (2002) 2625–2633.
[37] T. Kaasgaard, C. Leidy, J.H. Crowe, O.G. Mouritsen, K. Jorgensen, Temperature-controlled structure and kinetics of ripple phases in one- and two-component supported lipid bilayers, Biophys. J. 85 (1) (2003) 350–360.
[38] M.C. Giocondi, C. Le Grimellec, Temperature dependence of the surface topography in dimyristoylphosphatidylcholine/distearoylphosphatidylcholine multibilayers, Biophys. J. 86 (4) (2004) 2218–2230.
[39] V.D. Gordon, P.A. Beales, Z. Zhao, C. Blake, F.C. MacKintosh, P.D. Olmsted, M.E. Cates, S.U. Egelhaaf, W.C.K. Poon, Lipid organization and the morphology of solid-like domains in phase-separating binary lipid membranes, J. Phys. Condens. Matter 18 (32) (2006) L415–L420.
[40] L. Li, J.X. Cheng, Coexisting stripe- and patch-shaped domains in giant unilamellar vesicles, Biochemistry 45 (39) (2006) 11819–11826.
[41] D. Scherfeld, N. Kahya, P. Schwille, Lipid dynamics and domain formation in model membranes composed of ternary mixtures of unsaturated and saturated phosphatidylcholines and cholesterol, Biophys. J. 85 (6) (2003) 3758–3768.
[42] P.A. Beales, V.D. Gordon, Z.J. Zhao, S.U. Egelhaaf, W.C.K. Poon, Solid-like domains in fluid membranes, J. Phys. Condens. Matter 17 (45) (2005) S3341–S3346.
[43] L.A. Bagatolli, E. Gratton, A correlation between lipid domain shape and binary phospholipid mixture composition in free standing bilayers: a two-photon fluorescence microscopy study, Biophys. J. 79 (1) (2000) 434–447.
[44] L.A. Bagatolli, E. Gratton, Two photon fluorescence microscopy of coexisting lipid domains in giant unilamellar vesicles of binary phospholipid mixtures, Biophys. J. 78 (1) (2000) 290–305.
[45] J. Korlach, P. Schwille, W.W. Webb, G.W. Feigenson, Characterization of lipid bilayer phases by confocal microscopy and fluorescence correlation spectroscopy, Proc. Natl. Acad. Sci. 96 (15) (1999) 8461–8466.
[46] S.D. Shoemaker, T.K. Vanderlick, Material studies of lipid vesicles in the L-alpha and L-alpha-gel coexistence regimes, Biophys. J. 84 (2) (2003) 998–1009.
[47] A.C. Simonsen, Spatio-temporal organization of spincoated supported model membranes, in: M.L.L.R. Faller, T. Jue, S.H. Risbud (Eds.), Handbook of Modern Biophysics: Biomembrane Frontiers. Nanostructures, Models and the Design of Life, Vol. 2, Humana Press/Springer, 2009, pp. 141–169.
[48] U. Bernchou, J.H. Ipsen, A.C. Simonsen, Growth of solid domains in model membranes: quantitative image analysis reveals a strong correlation between domain shape and spatial position, J. Phys. Chem. B 113 (20) (2009) 7170–7177.
[49] J.F. Nagle, S. Tristram-Nagle, Structure of lipid bilayers, Biochim. Biophys. Acta, Rev. Biomembr. 1469 (3) (2000) 159–195.
[50] A. Schafer, T. Salditt, M.C. Rheinstadter, Atomic force microscopy study of thick lamellar stacks of phospholipid bilayers, Phys. Rev. E 77 (2) (2008) 8.
[51] K. Sengupta, V.A. Raghunathan, J. Katsaras, Structure of the ripple phase of phospholipid multibilayers, Phys. Rev. E 68 (3) (2003) 12.
[52] A.C. Simonsen, U.B. Jensen, P.L. Hansen, Hydrolysis of fluid supported membrane islands by phospholipase A(2): time-lapse imaging and kinetic analysis, J. Colloid Interface Sci. 301 (1) (2006) 107–115.
[53] M.H. Jensen, E.J. Morris, A.C. Simonsen, Domain shapes, coarsening, and random patterns in ternary membranes, Langmuir 23 (15) (2007) 8135–8141.
[54] A.C. Simonsen, Activation of phospholipase A(2) by ternary model membranes, Biophys. J. 94 (10) (2008) 3966–3975.
[55] U.B. Jensen, A.C. Simonsen, Shape relaxations in a fluid supported membrane during hydrolysis by phospholipase A(2), Biochim. Biophys. Acta, Biomembr. 1715 (1) (2005) 1–5.
[56] H.M. Seeger, M. Fidorra, T. Heimburg, Domain size and fluctuations at domain interfaces in lipid mixtures, Macromol. Symp. 219 (2004) 85–96.
[57] D. Keller, N.B. Larsen, I.M. Moller, O.G. Mouritsen, Decoupled phase transitions and grain-boundary melting in supported phospholipid bilayers, Phys. Rev. Lett. 94 (2) (2005) 025701.
[58] L.M.S. Loura, A. Fedorov, M. Prieto, Partitioning of membrane probes in a gel/fluid two-component lipid system: a fluorescence resonance energy transfer study, Biochim. Biophys. Acta 1467 (1) (2000) 101–112.
[59] C.H. Spink, M.D. Yeager, G.W. Feigenson, Partitioning behavior of indocarbocyanine probes between coexisting gel and fluid phases in mode membranes, Biochim. Biophys. Acta 1023 (1) (1990) 25–33.
[60] M. Fidorra, L. Duelund, C. Leidy, A.C. Simonsen, L.A. Bagatolli, Absence of fluid-ordered/fluid-disordered phase coexistence in ceramide/popc mixtures containing cholesterol, Biophys. J. 90 (12) (2006) 4437–4451.
[61] K. Sengupta, V. Raghunathan, Y. Hatwalne, Role of tilt order in the asymmetric ripple phase of phospholipid bilayers, Phys. Rev. Lett. 87 (5) (2001) 055705.
[62] U. Bernchou, J.R. Brewer, H.S. Midtiby, J.H. Ipsen, L.A. Bagatolli, A.C. Simonsen, Texture of lipid bilayer domains, J. Am. Chem. Soc. Commun. 131 (40) (2009) 14130+.
[63] N. Nandi, D. Vollhardt, Effect of molecular chirality on the morphology of biomimetic Langmuir monolayers, Chem. Rev. 103 (10) (2003) 4033–4075.
[64] W. Vaz, E. Melo, T. Thompson, Translational diffusion and fluid domain connectivity in a 2-component, 2-phase phospholipid-bilayer, Biophys. J. 56 (5) (1989) 869–876.